doi:10.1093/brain/awh531 *Brain* (2005), **128,** 1778–1789

LPS receptor (CD14): a receptor for phagocytosis of Alzheimer's amyloid peptide

Yang Liu,[1] Silke Walter,[1,*] Massimiliano Stagi,[3,4,*] Dmitry Cherny,[7,8] Maryse Letiembre,[1] Walter Schulz-Schaeffer,[2] Holger Heine,[5] Botond Penke,[9] Harald Neumann[3,4] and Klaus Fassbender[6]

[1]Departments of Neurology and [2]Neuropathology, University of Göttingen, [3]European Neuroscience Institute and [4]Institute of Multiple Sclerosis Research, University of Göttingen and Hertie-Foundation, Göttingen, [5]Borstel Research Centre, Centre for Medicine and Biosciences, Borstel, [6]Department of Neurology, University Hospital, Homburg, Saar, Germany, [7]Department of Biochemistry, University of Leicester, Leicester, UK, [8]Institute of Molecular Genetics, Russian Academy of Sciences, Moscow, Russia and [9]Department of Medical Chemistry, Albert Szent Gyorgyi Medical University, Szeged, Hungary

Correspondence to: Yang Liu or Klaus Fassbender, Department of Neurology, University of Göttingen, Robert Koch Str. 40, 37075 Göttingen, Germany
E-mail: alexliu@med.uni-goettingen.de; klaus.fassbender@med.uni-goettingen.de
*These authors contributed equally to this work.

The amyloid β peptide 42 ($A\beta_{42}$) plays a key role in neurotoxicity in Alzheimer's disease. Mononuclear phagocytes, i.e. microglia, have the potential to clear Aβ by phagocytosis. Recently, the lipopolysaccharide (LPS) receptor CD14 was shown to mediate phagocytosis of bacterial components and furthermore to contribute to neuroinflammation in Alzheimer's disease. Here, we investigated whether this key innate immunity receptor can interact with $A\beta_{42}$ and mediate phagocytosis of this peptide. Using flow cytometry, confocal microscopy and two-photon fluorescence lifetime imaging (FLIM) combined with fluorescence resonance energy transfer (FRET), we demonstrated a direct molecular interaction in the range of a few nanometers between $A\beta_{42}$ and CD14 in human CD14-transfected Chinese hamster ovary cells. Investigations using cells that were genetically deficient for this receptor showed that in <30 minutes exogenous $A\beta_{42}$ added to cultured primary microglial cells was phagocytosed into the cytoplasmic compartment in a CD14-dependent manner. This phagocytosis occurred at $A\beta_{42}$ concentration ranges that were considerably lower than the threshold to activate a cellular inflammatory reaction. In contrast, there was no association of CD14 to microglial internalization of microbeads. In complementary clinical experiments, we detected a pronounced CD14 immunoreactivity on parenchymal microglia spatially correlated to characteristic Alzheimer's disease lesion sites in brain sections of Alzheimer's disease patients but not in brain sections of control subjects. By showing a close interaction between CD14 and $A\beta_{42}$, demonstrating a direct role of CD14 in $A\beta_{42}$ phagocytosis, and detecting CD14-specific staining in brains of Alzheimer's disease patients, our results indicate a role of the LPS receptor in the pathophysiology of Alzheimer's disease, which could be of therapeutic relevance.

Keywords: Alzheimer's disease; amyloid β protein; CD14; microglia; phagocytosis

Abbreviations: Aβ = amyloid β peptide; CHO = Chinese hamster ovary; $fA\beta_{42}$ = fibrillar amyloid β peptide 42; FLIM = fluorescence lifetime imaging; FRET = fluorescence resonance energy transfer; iNOS = inducible nitric oxide synthase; LPS = lipopolysaccharide; mFI = mean fluorescence value; SEM = standard error of the mean; TCSPC = time-correlated single photon counting; TNF-α = tumour necrosis factor-α

Advance Access publication April 27, 2005

Introduction

Alzheimer's disease is a progressive neurodegenerative disease characterized by extracellular senile plaques and intracellular neurofibrillar tangles in the brain tissue. Amyloid β peptide (Aβ) is the main component of the senile plaques. Aβ has been shown to injure neurons both directly and indirectly, via induction of chronic neuroinflammatory response (Games *et al.*, 1995; McGeer and McGeer, 2003; Nicoll *et al.*, 2003).

Since deposition of the 42 kD form of Aβ ($A\beta_{42}$) is considered to be a key pathogenic event in Alzheimer's disease, its removal is desirable (Citron, 2002). Very little is known about

the molecular mechanism of endocytic or phagocytic clearance of Aβ peptide. Recently, immunotherapy directed against Aβ as a way to eliminate this key molecule of Alzheimer's disease has gained much interest. Vaccination against Aβ in a mouse model of Alzheimer's disease indeed reduced Aβ plaques and prevented cognitive deficits (Bard *et al.*, 2000; Janus *et al.*, 2000). One hypothesis proposed that antibodies directed against Aβ trigger microglial cells to clear plaques through phagocytosis and subsequent peptide degradation (Bard *et al.*, 2000). However, a clinical trial in which Alzheimer's disease patients were vaccinated with Aβ had to be discontinued after several patients experienced meningoencephalitis (Check, 2002). Moreover, the specificity of plaque removal by Aβ immunotherapy was recently questioned because non-specific microglial activation already appears to be sufficient to phagocytose Aβ fibrils (Akiyama and McGeer, 2004).

CD14, a 55-kD glycosylphosphatidyl inositol (GPI)-anchored surface myeloid glycoprotein, is expressed on microglial cells and is responsible for uptake of bacterial component lipopolysaccharide (LPS) via macropinocytosis (Poussin *et al.*, 1998; Vasselon *et al.*, 1999). CD14-dependent phagocytosis by mononuclear phagocytes has also been demonstrated for *Mycobacterium tuberculosis* (Peterson *et al.*, 1995), *Actinobacillus actinomycetemcomitans* (Muro *et al.*, 1997), *Cryptococcus neoformans* (Lipovsky *et al.*, 1997), apoptotic cells (Devitt *et al.*, 1998) and atherogenic lipids (Schmitz and Orso, 2002).

We recently showed that CD14 plays a role in microglial activation by $A\beta_{42}$ (Fassbender *et al.*, 2004). Since CD14 has been recognized to be involved in both cellular inflammatory activation by microbial components and pathogen internalization, we asked whether CD14 could be important in microglial phagocytosis of Aβ.

Material and methods

Characterization of $A\beta_{42}$ peptides by electron microscopy

Biotinylated $A\beta_{42}$ peptide (human amyloid β peptide 1–42 conjugated at the N-terminus with biotin) was purchased from Bachem (Heidelberg, Germany) and unconjugated $A\beta_{42}$ was a gift from B. Penke (Albert Szent Gyorgyi Medical University, Szeged, Hungary). Fibrillar $A\beta_{42}$ ($fA\beta_{42}$) was obtained by dissolving the synthetic human peptide in 1× phosphate-buffered saline (PBS) (1 mg/ml) and incubating it for 7 days at 37°C. Endotoxin concentrations of stock peptide samples were <0.01 EU/ml as determined by the Limulus Amebocyte Lysate assay system (Cambrex, Verviers, Belgium) according to the manufacturer's instructions.

Peptide samples of $fA\beta_{42}$ and biotinylated $fA\beta_{42}$ were prepared for electron microscopic examination as described previously (Hoyer *et al.*, 2002). Briefly, peptide samples were diluted 20–30 fold in 10 mM Tris–HCl, 10 mM NaCl, pH 7.5 and placed on a glow-discharged carbon film attached to an electron microscopy grid. After 1 min of adsorption, the grids were stained with a few drops of 2% aqueous uranyl acetate, blotted with filter paper and dried. The samples were examined with a Philips CM12 electron microscope (Philips, Eindhoven, the Netherlands) in a bright-field mode. Measurements of the micrographs were carried out with the Windows version of NIH Image software (Scion Corporation, Frederick, MA, USA).

Primary microglial and CHO cell culture

Microglial cells were prepared from brains of postnatal (P1–P3) C57BL/6J (CD14wt) and CD14-deficient (CD14ko) mice obtained from The Jackson Laboratory (Bar Harbor, Maine, USA). CD14ko mice have been backcrossed into C57BL/6J for at least six generations (Moore *et al.*, 2000). Briefly, meninges were mechanically removed and the cells were cultured in Dulbecco's Modified Eagle's Medium (DMEM) (GibcoBRL, Eggenstein, Germany) supplemented with 10% fetal calf serum (FCS) (PAA Laboratories, Cölbe, Germany) under a humidified atmosphere of 10% CO_2 at 37°C for at least 14 days (Ishii *et al.*, 2000). To collect microglial cells, the microglia–astrocyte co-cultures were shaken on a rotary shaker (220 r.p.m.) for 2 h.

Chinese hamster ovary (CHO) cells stably transfected with pCEP4-huCD14 (CHO-CD14) (kindly provided by H. Heine, Borstel Research Centre, Centre for Medicine and Biosciences, Borstel, Germany) (Golenbock *et al.*, 1993) were cultured in Ham's F12 medium (GibcoBRL) supplemented with 10% FCS (PAA Laboratories) at 37°C in a humidified incubator under 10% CO_2.

FRET analysis of the proximity between $fA\beta_{42}$ and CD14 using FLIM and TCSPC

Fluorescence resonance energy transfer (FRET) measurements were applied to investigate the proximity at a nanometer scale between $fA\beta_{42}$ and CD14. Fluorescence lifetime imaging (FLIM) was performed, which relies on the fluorescence lifetime measurement (the time of fluorophore emission measured in picoseconds after brief femtosecond excitation). Lifetime of a donor decreases in the presence of an appropriate FRET acceptor. To record fluorescence lifetime images, time-correlated single photon counting (TCSPC) was used, which has high intrinsic time resolution and accuracy as well as high counting efficiency, both of which are required to resolve multi-exponential decay analysis in scanning microscope (Bacskai *et al.*, 2003).

The set-up used in this study consisted of a laser scanning microscope (Leica, Bensheim, Germany) equipped with a femtosecond pulsed two-photon laser (Coherent, Dieburg, Germany) and connected to a TCSPC imaging module (SPC, Becker & Hickl, Berlin, Germany). The data analysis software (SPCImage, Becker & Hickl) allowed multi-exponential curve fitting of the acquired data on a pixel-by-pixel basis using a weighted least-squares numerical approach.

The CHO-CD14 cells cultured in chamber slides (Nunc Lab, Wiesbaden, Germany) were treated with 10 μg/ml fAβ42 for 1 h. The cells were then stained and analysed by confocal microscopy and lifetime measurement. Confocal and lifetime images were collected from five different samples:

(i) as a control, biotinylated $fA\beta_{42}$ (10 μg/ml) treated CHO-CD14 cells stained by mouse anti-human CD14 (RMO52, Beckman Coulter, Marseille, France) and secondary Alexa488-conjugated donkey anti-mouse IgG (Molecular Probes, Leiden, the Netherlands), but without Cy3-conjugated streptavidin;
(ii) biotinylated $fA\beta_{42}$ treated CHO-CD14 cells stained by primary mouse anti-human CD14 and Alexa488–conjugated secondary

antibodies and Cy3-conjugated streptavidin (Amersham, Freiburg, Germany);

(iii) as a protein control, biotinylated bovine serum albumin (10 μg/ml, Sigma, Taufkirchen, Germany) treated CHO-CD14 cells stained by primary mouse anti-human CD14 and Alexa488–conjugated secondary antibodies and Cy3-conjugated streptavidin;

(iv) as a receptor control, biotinylated $fA\beta_{42}$-treated CHO-CD14 cells stained by primary rat anti-mouse CD44 antibody (KM114, Pharmingen, Heidelberg, Germany) which cross-reacts with CD44 of Chinese hamster (Katoh *et al.*, 1995) and secondary Alexa488-conjugated donkey anti-rat IgG (Molecular Probes) and Cy3-conjugated streptavidin;

(v) as a FRET positive control, biotinylated $fA\beta_{42}$-treated CHO-CD14 cells stained by primary mouse anti-human CD14 and secondary Cy3-conjugated goat anti-mouse IgG (Jackson ImmunoResearch Laboratories, West Grove, PA, USA) and then further treated with Alexa488-conjugated donkey anti-goat IgG (Molecular Probes).

The lifetime of Alexa488 was visualized by coding the FLIM-signal in pseudocolours on a pixel-by-pixel basis over the entire image. The measured lifetime of Alexa488 in the ranges of 500∼1800 and 1800∼4000 picoseconds were coded with red and blue colours, respectively. The lifetimes were showed simultaneously in histograms and quantified by calculating the ratios of pixel counts in the ranges of 500∼1800 and 1800∼4000 picoseconds from each sample.

Laser scanning confocal microscopy analysis of $fA\beta_{42}$ internalization into primary microglia

CD14wt and CD14ko microglial cells grown on chamber slides were treated with 0.25, 2.5 or 25 μg/ml biotinylated $fA\beta_{42}$ for 5, 30, 60 or 120 min in microglial culture medium at 37°C and 10% CO_2.

To demonstrate that uptake of $fA\beta_{42}$ involves phagocytosis, microglial cells were pretreated with 5 μM cytochalasin D (Sigma, Taufkirchen, Germany) for 1 h, prior to exposure to 2.5 μg/ml biotinylated $fA\beta_{42}$ for 1 h. The cells were fixed in 4% paraformaldehyde and then permeabilized with 0.2% Triton-100. After blocking with 10% normal serum, microglial cells were incubated overnight at 4°C with rat anti-mouse LAMP-2 monoclonal antibody (obtained from ABL-93 hybridoma cell culture, Development Studies Hybridoma Bank, Department of Biological Sciences, University of Iowa, IA, USA) (Chen *et al.*, 1985). After rinsing, slides were incubated for 1 h at room temperature with Cy5-conjugated goat anti-rat IgG (Jackson ImmunoResearch Laboratories).

Microglial cells were further treated with FITC conjugated rat anti-mouse CD14 (rmC5-3, Pharmingen) for 1 h at room temperature. After rinsing, slides were incubated with Alexa488 conjugated rabbit anti-FITC IgG (Molecular Probes) and Cy3-conjugated streptavidin (Amersham). The slides were mounted with mowiol and kept at 4°C in the dark until analysis under a laser scanning confocal microscopy (Leica LSC, Heidelberg, Germany). Images of microglia treated with isotype control primary antibodies were used to assess background fluorescence. Under confocal microscopy, at least five areas containing >200 cells were randomly chosen according to LAMP-2 staining, indicating the numbers of total cells. The numbers of microglia containing engulfed $fA\beta_{42}$ were determined by counting cells with Cy3 internalization. The percentage of $fA\beta_{42}$-internalized microglia was shown as the mean and standard error of the mean (SEM) from at least three independent experiments.

Flow cytometry analysis of $fA\beta_{42}$ and polystyrene microsphere internalization

After culturing on 24-well plates (BD Falcon, Heidelberg, Germany), CD14wt and CD14ko microglial cells were incubated with 2.5 μg/ml biotinylated $fA\beta_{42}$ or 1 μl/ml (1×10^7 fluorescent polystyrene microspheres, 1-μm diameter) stock solution of yellow-green FluoSpheres Fluorescent Microspheres (YG beads; Molecular Probes) in culture medium for 1 h. The internalization assay was terminated by placing cells on ice. Cells were washed four times with ice-cold 1× PBS to remove residual unbound $fA\beta_{42}$ or microspheres, and then detached from the bottom of the wells by treatment with trypsin-EDTA (GibcoBRL) at 4°C. Microsphere treated cells were directly and immediately analysed by flow cytometry. The $fA\beta_{42}$-treated cells were fixed and permeabilized with Cytofix/Cytoperm Kit (BD Falcon) according to the manufacturer's instructions. The cells were incubated with FITC-conjugated streptavidin (Amersham) for 2 h at room temperature. After washing, the samples were analyzed by flow cytometry. Control cells for extracellular surface binding of biotinylated $fA\beta_{42}$ and microspheres were incubated with 2.5 μg/ml biotinylated $fA\beta_{42}$ or 1 μl/ml stock solution of YG beads for 1 h on the ice. The mean fluorescence value (mFI) for internalization of $fA\beta_{42}$ or YG beads in each sample was determined. All experiments were independently replicated at least three times. Means and SEM of three independent experiments were compared using independent-samples *t*-test on SPSS 11.0 for Windows (SPSS Inc, Chicago, USA).

Reverse transcription and quantitative PCR for analysis of inflammatory and CD14 gene transcripts

CD14wt microglial cells grown on 24-well plate were stimulated with 0.25, 2.5 and 25 μg/ml biotinylated $fA\beta_{42}$ for 1 h in culture medium at 37°C and 10% CO_2. LPS from *E.coli* (Sigma) was used as a positive control. Total RNA was isolated from microglia by the RNEasy Mini Kit (Qiagen, Hilden, Germany).

First-strand cDNA was synthesized by priming total RNA with hexamer random primers (Roche Molecular Biochemicals, Mannheim, Germany) and using Superscript III reverse transcriptase according to the manufacturer's instructions (Invitrogen, Karlsruhe, Germany).

For quantification, real-time quantitative PCR was performed using the Applied Biosystems GeneAmp® 5700 Sequence Detection System (Applied Biosystems, Foster City, USA). The following oligonucleotides (Invitrogen, Karlsruhe, Germany) were used for PCR amplification: GAPDH forward: 5′-ACAACTTTGGCATTGTGGAACTTTGGCATTGTGGAA-3′, reverse: 5′-GATGCAGGGATGATGTTCTG-3′; tumour necrosis factor-α (TNF-α) forward: 5′-ATGAGAAGTTCCCAAATGGC-3′, reverse: 5′-CTCCACTTGGTGGTTTGCTA-3′; inducible nitric oxide synthase (iNOS) forward: 5′-ACCTTGTTCAGCTACGCCTT-3′, reverse: 5′-CATTCCCAAATGTGCTTGTC-3′ and CD14 forward: 5′-AGGGTACAGCTGCAAGGACT-3′, reverse: 5′-CTTCAGCCCAGTGAAAGACA-3′.

The amount of double-stranded PCR product synthesized in each cycle was measured using SYBR green I dye. Threshold cycle (Ct) values for each inflammatory gene from the replicate PCRs was normalized to the Ct values for the GAPDH control from the same cDNA preparations. The ratio of transcription of each gene was calculated as $2^{(\Delta Ct)}$, where ΔCt is given by: Ct(test gene) – Ct(GAPDH).

Immunohistochemical analysis of CD14 in Alzheimer's disease brains

Archival, formalin-fixed and paraffin-embedded autopsy tissue blocks from human frontal, occipital cortex and hippocampus from patients with histologically confirmed Alzheimer's disease and from age-matched non-demented control subjects were retrieved from the Department of Neuropathology, University of Göttingen, Germany. Slides were pre-treated as follows: microwave heating for 7 × 5 min in citrate buffer pH 6.0, followed by treatment with formic acid for 1 min. The endogenous peroxidase was then quenched by the treatment with 3% H_2O_2 in 1× PBS. The slides were incubated with 4 M guanidine thiocyanate (Amresco, Solon, Ohio, OH, USA) for 15 min with washing steps in between.

Sections were blocked with 0.5% casein for 1 h. Staining was performed using the mouse monoclonal antibody against human CD14 (1:100, NCL-L-CD14-223, Novocastra, Newcastle-upon-Tyne, UK) followed by alkaline phosphatase (AP)-conjugated goat anti-mouse IgG antibody (1:500, DAKO, Hamburg, Germany). The substrate for the development of AP consisted of 6.3 μl of 5% (w/v) neufuchsin (Sigma) in 16 μl of 4% sodium nitrite (Fluka, Kassel, Germany), 2 mg of naphthol-ASBi-phosphate (Sigma) in 20 μl of N,N-dimethylformamide (Merck, Darmstadt, Germany), and 3 ml of 0.05 M Tris–HCl buffer pH 8.7 containing 1 mM levamisole (Sigma). The slides were thereafter incubated overnight at 4°C with rabbit polyclonal antiserum 730 against human Aβ (1:50, gift from G. Multhaup, ZMBH, University of Heidelberg, Germany) (Borchardt *et al.*, 1999) diluted in 1× PBS. After washes, horseradish peroxidase (HRP)-conjugated goat anti-rabbit IgG antibody (1:100, DAKO) was applied before development with 0.5 mg/ml 3,3′-diaminobenzidine tetrahydrochloride (DAB) (Sigma) and 0.0003% H_2O_2 in 1× PBS. The slides were counter-stained with haematoxylin. Since there is currently no single marker to distinguish microglia and macrophage, we identified microglia by their characteristic ramified morphology, elongated or irregular nucleus and location in the neural parenchyma.

Results

Fibril formation by biotinylated $A\beta_{42}$ peptide

$A\beta_{42}$ peptide conjugated with biotin (biotinylated $A\beta_{42}$) was used in this study to allow direct analysis of $A\beta_{42}$. We first confirmed that biotinylated $A\beta_{42}$ forms fibrils *in vitro*, as does unconjugated $A\beta_{42}$, by transmission electron microscopy. Both normal $fA\beta_{42}$ and biotinylated $fA\beta_{42}$ showed thin elongated fibrils (Fig. 1A and B). The fibrils formed by biotinylated $A\beta_{42}$ were approximately half the length of unconjugated $A\beta_{42}$ fibrils (~200–300 nm), but had the same width of 7 nm (Fig. 1A and B). Thus, the biotinylated $A\beta_{42}$ fibrils used in the following experiments were very similar in structure to the unconjugated $A\beta_{42}$ fibrils.

Molecular interaction between $fA\beta_{42}$ and CD14

To study the molecular interaction between $fA\beta_{42}$ and CD14, CHO cells were stably transfected with human CD14 (CHO-CD14) and the proximity between the two molecules was analysed by FLIM-based FRET. FRET can occur between a fluorescent donor and a corresponding fluorescent acceptor molecule if the distance between the two fluorophores is less than the R0 (the characteristic Förster distance at which FRET efficiency is 0.5, i.e. the state in which exactly half of the energy are transferred from the donor to the acceptor). The Förster distance can be calculated directly from the spectral properties of the dyes and typically lies between 1 and 10 nm (Stryer, 1978).

FLIM analysis of $fA\beta_{42}$-treated CHO-CD14 cells stained with Alexa488-labelled anti-CD14 antibody as the FRET donor was performed first without specific labelling of $fA\beta_{42}$ to determine the normal lifetime of Alexa488. Alexa488-labelled CD14 was detected by confocal microscopy throughout the cells (Fig. 2A). In most of the pseudocoloured FLIM images, the lifetime of Alexa488-labelled CD14 was >1800 picoseconds (coded in blue in Fig. 2C) and showed a single distribution with a peak at 2350 picoseconds (Fig. 3A).

When biotinylated $fA\beta_{42}$ on treated CHO-CD14 cells was visualized with Cy3-conjugated streptavidin, biotinylated $fA\beta_{42}$ was detected on the cell membrane and within CHO-CD14 cells by confocal microscopy (Fig. 2F). With Cy3-labelled $fA\beta_{42}$ as the FRET acceptor, the lifetime of Alexa488 on CD14 shifted to <1800 picoseconds (coded in

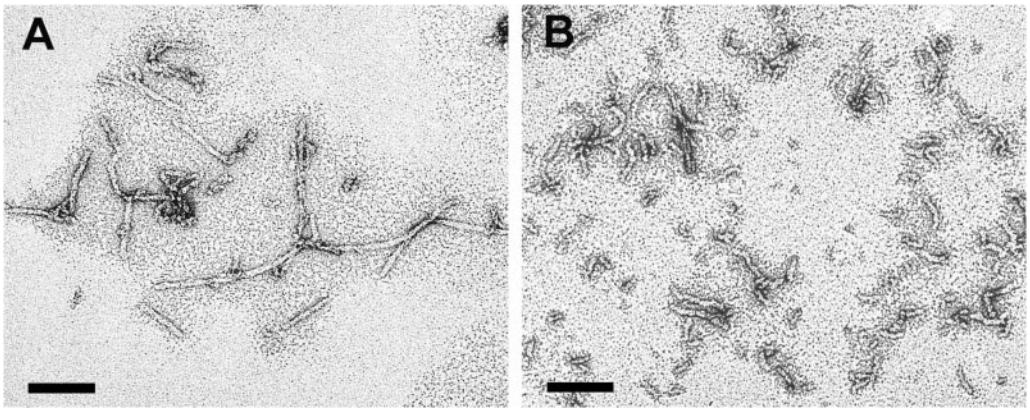

Fig. 1 Electron microscopic analysis of $A\beta_{42}$ fibrils. The electron microscope images demonstrate the aggregated conformation of both unconjugated (**A**) and biotinylated (**B**) $A\beta_{42}$ (negative staining). Unconjugated $A\beta_{42}$ (**A**) forms fibrils of ~7 nm width and ~200–300 nm length whereas biotinylated $A\beta_{42}$ (**B**) formed fibrils of ~7 nm width and ~20–150 nm length. Scale bars: 100 nm.

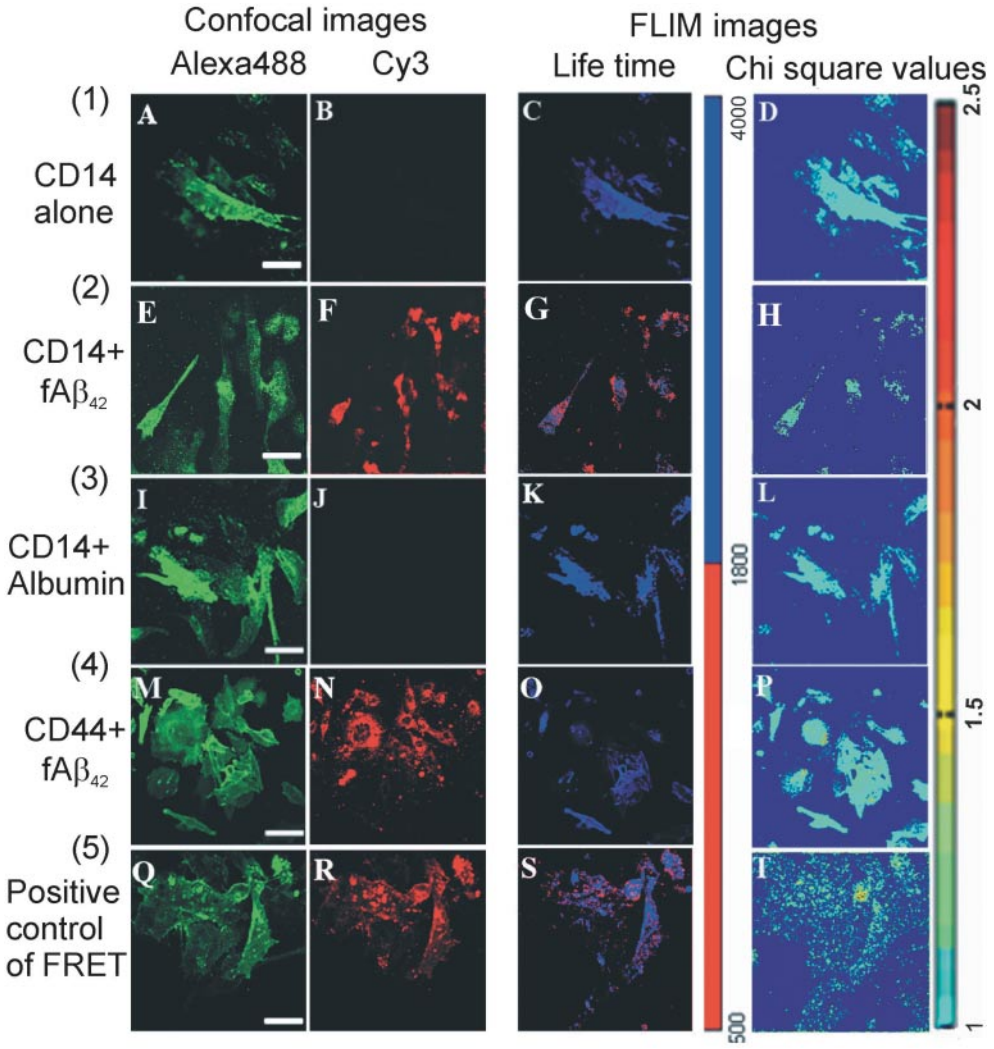

Fig. 2 Confocal and FLIM image analysis of fAβ_{42} and CD14 molecules. Confocal images show immunostaining for CD14 (**A**, **E**, **I**), CD44 (**M**), biotinylated fAβ_{42} (**F**, **N**) and biotinylated albumin (**J**). The pseudocoloured FLIM images indicate the lifetimes of Alexa488-conjugated antibodies directed against CD14 (**C**, **G**, **K**) or CD44 (**O**). The lifetime is >1800 picoseconds (blue) (**C**, **K**, **O**) in areas without FRET and <1800 picoseconds (red) (**G**, **S**) in areas exhibiting FRET. The areas (**G**) exhibiting the closest distance between fAβ_{42} and CD14 are located both on the cell surface and intracellularly in vesicular-like structures. Control FLIM images with biotinylated albumin instead of fAβ_{42} show no shift of lifetime of Alexa488 (**K**). Control FLIM images of CD44 staining and fAβ_{42} treatment show no shift of lifetime of Alexa488 (**O**). In the positive FRET control, the lifetime of Alexa488 is strongly reduced (**S**). χ^2 values for the corresponding FLIM images are coded in pseudocolours (**D**, **H**, **L**, **P**, **T**). χ^2 values are all <2.5 indicating the reliability of the measured lifetimes. Scale bars: 10 μm.

red), indicating a molecular interaction between Aβ_{42} and CD14 (Fig. 2G and Fig. 3B).

As a peptide control of the interaction specificity, CHO-CD14 cells were incubated with biotinylated bovine albumin instead of biotinylated fAβ_{42}. No Cy3-albumin staining could be observed by confocal microscopy (Fig. 2J) and the lifetime of Alexa488 (Fig. 2K and Fig. 3C) was not shifted, demonstrating a lack of any interaction between biotinylated bovine albumin and CD14.

To show that biotinylated fAβ_{42} does not bind non-specifically to cell surface receptors, CHO-CD14 cells treated with biotinylated fAβ_{42} were stained for CD44 as a constitutively expressed control receptor (Fig. 2 M). No shift of lifetime of Alexa488 on CD44 could be observed (Fig. 2O and Fig. 3D), demonstrating that fAβ_{42} does not interact with CD44.

To quantify the shift in the lifetime of Alexa488 due to FRET, we calculated the ratio of pixel count of short lifetimes (500∼1800 picoseconds) to that of long lifetimes (1800∼4000 picoseconds) of individual cells. The ratio increased significantly from 38.6 ± 9.1% to 73.8 ± 2.4% (mean ± SEM) in Alexa488-CD14 plus Cy3-Aβ_{42} labelled sample compared with only Alexa488-CD14 labelled control sample (Fig. 3F) ($n = 5$; independent-samples t test, $t = -4.8$, $P = 0.001$). The shift of the lifetime due to molecular interaction between Cy3-Aβ_{42} and Alexa488-CD14 was relatively strong compared with a FRET positive control where Cy3-conjugated antibody was directly bound to Alexa488-labelled antibody (Fig. 3F).

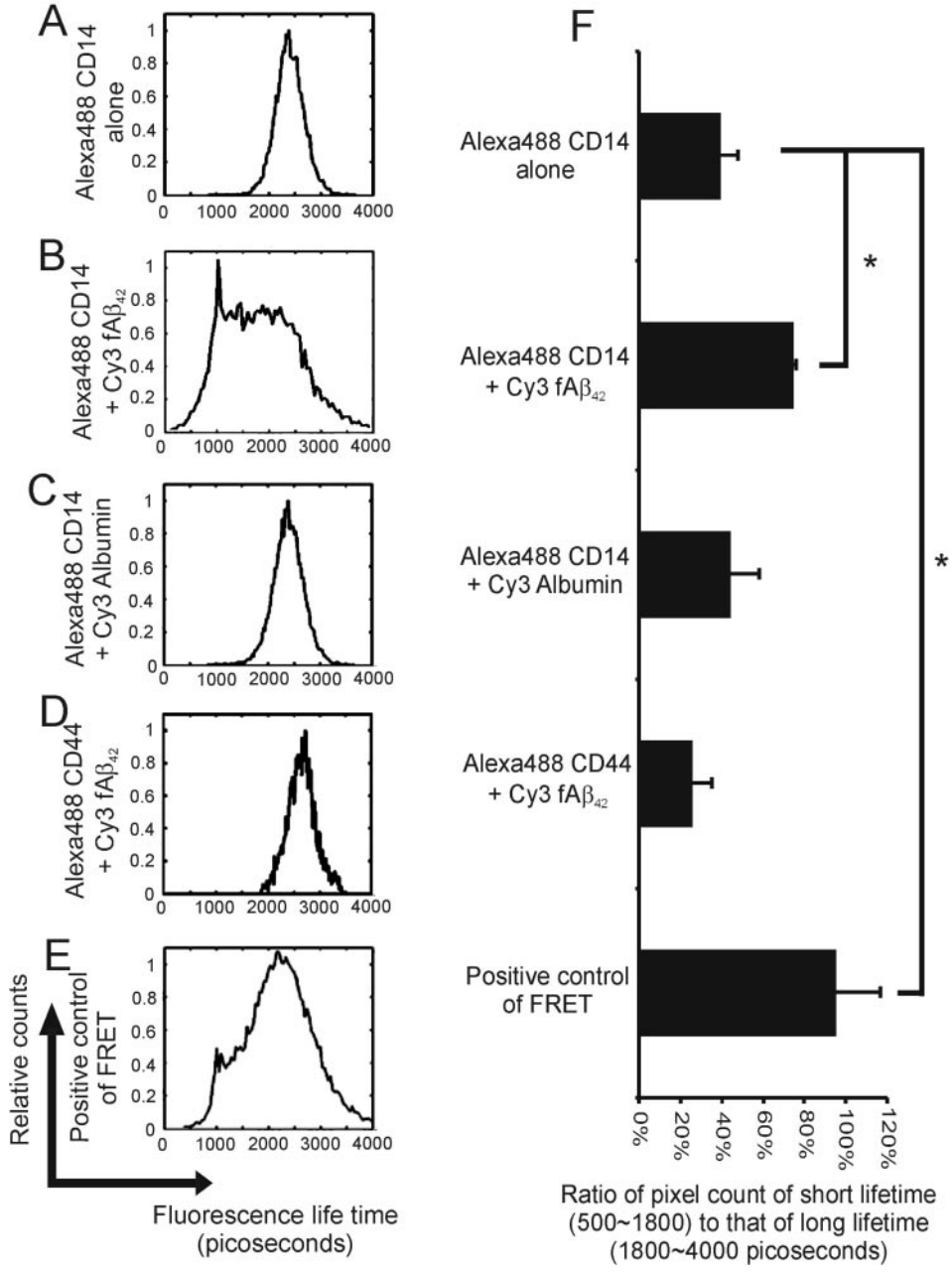

Fig. 3 Analysis of fluorescence lifetime distribution. FRET between Alexa488-stained CD14 and Cy3-stained biotinylated $A\beta_{42}$ can be detected through a shortening of the Alexa488 (FRET donor) fluorescence lifetime measured by FLIM. The lifetime distribution of Alexa488-CD14 is shown under control conditions (without staining of $A\beta_{42}$), as a normal distribution with a peak at ~2350 picoseconds (**A**). In contrast, with Cy3-stained biotinylated $A\beta_{42}$ as an acceptor of FRET, the lifetime is reduced to <1800 picoseconds (**B**). No shift of Alexa488 lifetime is detected with Cy3-albumin as a FRET acceptor, when biotinylated albumin was added instead of $A\beta_{42}$ (**C**). Furthermore, no shift of Alexa488 lifetime is detected when Alexa488-stained CD44 was used as a donor and Cy3-stained $A\beta_{42}$ as the acceptor (**D**). The lifetime of Alexa488 is markedly reduced with a FRET positive control (**E**). The shift in lifetime is quantified by determination of the ratio of pixel count of short lifetimes (500~1800) to that of long lifetimes (1800~4000 picoseconds). The ratio of the pair of Alexa488-stained CD14 and Cy3-stained $A\beta_{42}$ is significantly higher than that of the control pair with Alexa488-stained CD14 and unstained $A\beta_{42}$ (*$P < 0.05$, $n = 5$, independent-samples *t*-test) (**F**). Data are presented as mean ± SEM from five different regions of interest of distinct cells for each experimental group.

$fA\beta_{42}$ internalization by microglial cells

Since microglia are the first resident brain cell type to react to the deposition of $fA\beta_{42}$, we investigated the role of CD14 on microglial cells in $fA\beta_{42}$ internalization. CD14 is constitutively expressed by microglia and up-regulated after stimulation in an *in vitro* culture system (data not shown) and human brain (described in the following section). Microglial cell cultures were treated with serial concentrations of

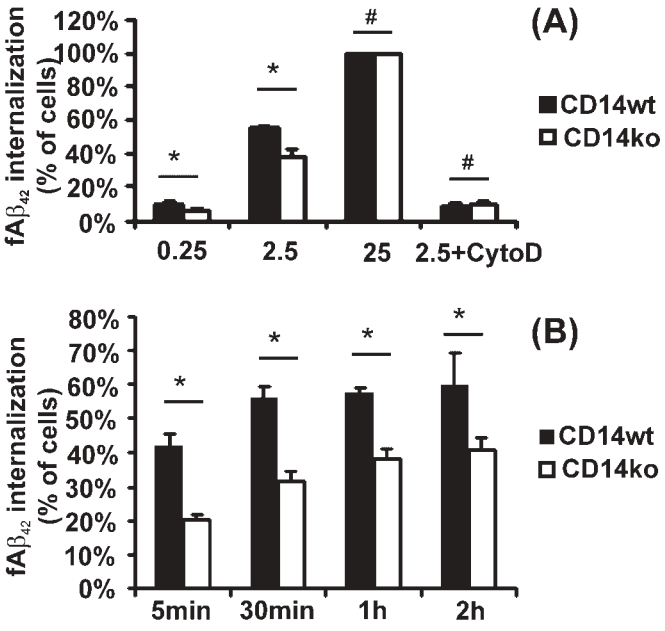

Fig. 4 Concentration-, time- and cytoskeleton-dependent internalization of $fA\beta_{42}$ in CD14wt and CD14ko microglia. The extent of $fA\beta_{42}$-internalization was determined by counting the number of microglia having internalized $fA\beta_{42}$ under laser scanning confocal microscopy. CD14wt and CD14ko microglia cultured on chamber slides were incubated with different concentrations of biotinylated $fA\beta_{42}$ (0.25, 2.5 and 25 μg/ml) (**A**) or with 2.5 μg/ml biotinylated $fA\beta_{42}$ for distinct time periods (5, 30, 60, 120 min) (**B**). To determine the role of the cytoskeleton in internalization of $fA\beta_{42}$, microglial cells were pre-treated for 1 h with 5 μM cytochalasin D (CytoD) and then incubated for 1 h with 2.5 μg/ml biotinylated $fA\beta_{42}$ (**A**). Data are shown as the mean ± SEM from three independent experiments. At $fA\beta_{42}$ concentrations of 0.25 and 2.5 μg/ml, a clear difference in $fA\beta_{42}$ internalization between CD14wt and CD14ko microglia was observed (*$P < 0.05$, $n = 3$, independent-samples *t*-test) (**A**, **B**). No change in $fA\beta_{42}$ internalization was detected if the concentration of $fA\beta_{42}$ was 25 μg/ml or if cytochalasin D was added (# $P > 0.05$, $n = 3$, independent-samples *t*-test) (**A**).

biotinylated $fA\beta_{42}$ to study uptake of $fA\beta_{42}$. The internalization of $fA\beta_{42}$ increased along with the $fA\beta_{42}$ peptide concentrations (0.25∼25 μg/ml) both in CD14wt and CD14ko microglia (Fig. 4A). Internalization within 1 h was more clearly detected at a concentration of 2.5 μg/ml $fA\beta_{42}$ instead of 0.25 μg/ml (Fig. 4A). $fA\beta_{42}$ (2.5 μg/ml) was then used to determine the kinetics of $fA\beta_{42}$ uptake. The kinetic study revealed that the internalization of $fA\beta_{42}$ increased over time after administration of the peptide (Fig. 4B). After 5 min, $fA\beta_{42}$ and CD14 co-localized at the surfaces of CD14wt microglia. Subsequently, this complex of $fA\beta_{42}$/CD14 was rapidly internalized and co-localized after 30 min with LAMP-2, a lysosomal marker (Fig. 5).

To test whether the internalization was of a phagocytic nature, we investigated the effects of cytochalasin D, a known inhibitor of phagocytosis (Mimura and Asano, 1976). When we applied 5 μM cytochalasin D 1 h before incubation with biotinylated $fA\beta_{42}$, the internalization of $fA\beta_{42}$ in both CD14wt and CD14ko microglia was almost completely inhibited (Fig. 4A), demonstrating that the internalization of $fA\beta_{42}$ occurred via phagocytosis.

CD14 facilitates internalization of $fA\beta_{42}$ by microglial cells

After observing that microglia phagocytose $A\beta_{42}$ fibrils was associated with CD14, we investigated whether CD14 is functionally relevant in microglial $fA\beta_{42}$ internalization. We compared the $fA\beta_{42}$ internalization in CD14wt and CD14ko microglia by counting microglia engulfing $A\beta_{42}$ fibrils under confocal microscopy and measuring mean fluorescence intensity by flow cytometry.

Under confocal microscopy, we observed that at 0.25 μg/ml biotinylated $fA\beta_{42}$, CD14wt microglia internalized significantly more $fA\beta_{42}$ within 1 h than did CD14ko microglia (9.34 ± 0.61% versus 5.99 ± 0.12% positive cells, respectively, mean ± SEM; $n = 3$; independent-samples *t* test: $t = 5.37$, $P = 0.028$) (Fig. 4A). At 2.5 μg/ml $fA\beta_{42}$, CD14wt microglia also internalized significantly more $A\beta_{42}$ fibrils than did CD14ko microglia at any of the time periods studied (Fig. 4B). The difference between CD14wt and CD14ko microglia in $fA\beta_{42}$ internalization was more pronounced at 5 min than at 2 h. For example at 5 min, CD14wt microglia phagocytosed considerably more $fA\beta_{42}$ than did CD14ko microglia (41.30 ± 2.29% versus 20.27 ± 1.53% positive cells, respectively, mean ± SEM; $n = 3$; independent-samples *t* test: $t = 8.56$, $P = 0.006$).

We confirmed these results with flow cytometry. CD14wt microglia internalized significantly more biotinylated $fA\beta_{42}$ than did CD14ko microglia (Fig. 6A and C). Within 1 h after incubation with biotinylated $fA\beta_{42}$, the mFI of CD14wt microglial cells was 54.19 ± 4.27 (mean ± SEM; $n = 4$), while that of CD14ko microglia was 37.16 ± 1.31 (mean ± SEM; $n = 4$) (Fig. 6C) (independent-samples *t* test: $t = 3.81$, $P = 0.023$). Pretreatment with cytochalasin D abrogated the internalization of $fA\beta_{42}$ in both cells, confirming the phagocytic manner of the internalization.

We next analysed whether CD14 modulates phagocytosis of microglial cells in general. Microglia readily internalized polystyrene microspheres (Fig. 6B and D). As expected, there was no significant difference in internalization of beads between CD14wt and CD14ko microglial cells (Fig. 6B and D) (mFI: 579.33 ± 53.36 versus 543.22 ± 41.68, respectively, mean ± SEM; $n = 3$; independent-samples *t* test: $t = -0.53$, $P = 0.61$).

Taken together, the results of these two experiments indicated that phagocytosis of biotinylated $fA\beta_{42}$ is strongly reduced in CD14ko microglia, whereas phagocytosis of beads is unaffected. In order to exclude the possibility that the reduced internalization of $fA\beta_{42}$ shown here was due to down-regulated expression of scavenger receptor (known to be a receptor for Aβ phagocytosis), we measured the gene transcript levels of scavenger receptor class A (SR-A) in CD14ko and CD14wt microglia by semi-quantitative RT-PCR. We did not observe any difference in SR-A gene

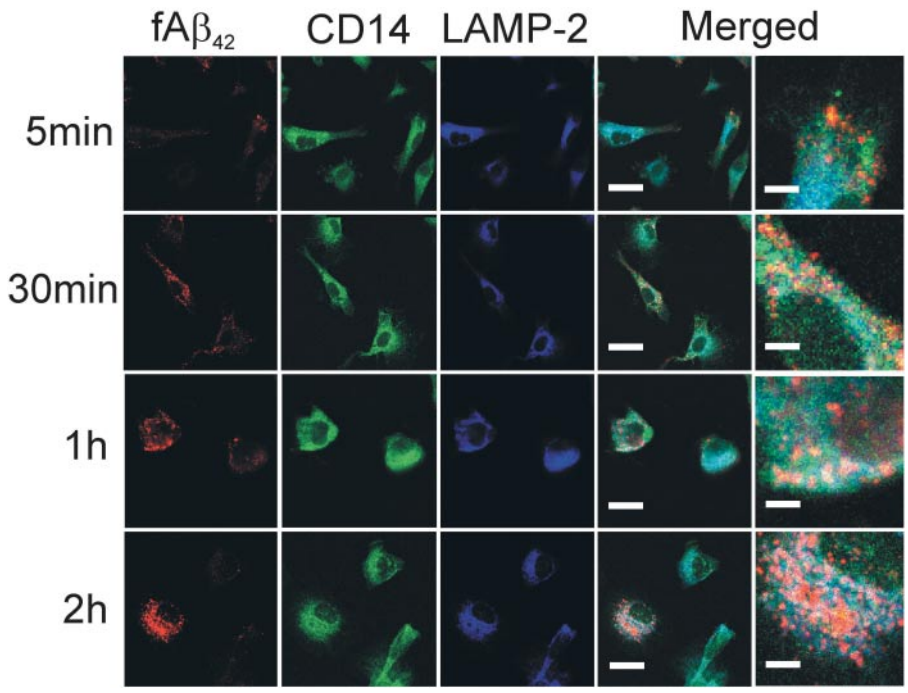

Fig. 5 Microglial internalization and co-localization of fAβ$_{42}$ to CD14. CD14wt microglia was treated with 2.5 μg/ml biotinylated fAβ$_{42}$ for distinct time periods (5, 30, 60, 120 min). The cells were stained with antibodies directed against the mouse lysosomal marker protein LAMP-2 and CD14, and then with Cy5 (blue) and Alexa488 (green) conjugated secondary antibodies, respectively. fAβ$_{42}$ was visualized with Cy3-conjugated streptavidin (red). Under confocal microscopy, co-localization of fAβ$_{42}$ and CD14 was shown by yellow fluorescence as a result of superimposing fluorescence images of fAβ$_{42}$ (red) and CD14 (green) within 5 min. This was followed by rapid internalization of fAβ$_{42}$ in conjugation with CD14 into lysosomes as demonstrated by a white fluorescence that results from superimposing the three fluorescence images. Scale bars: 10 μm (low magnification images) and 2.5 μm (high magnification images).

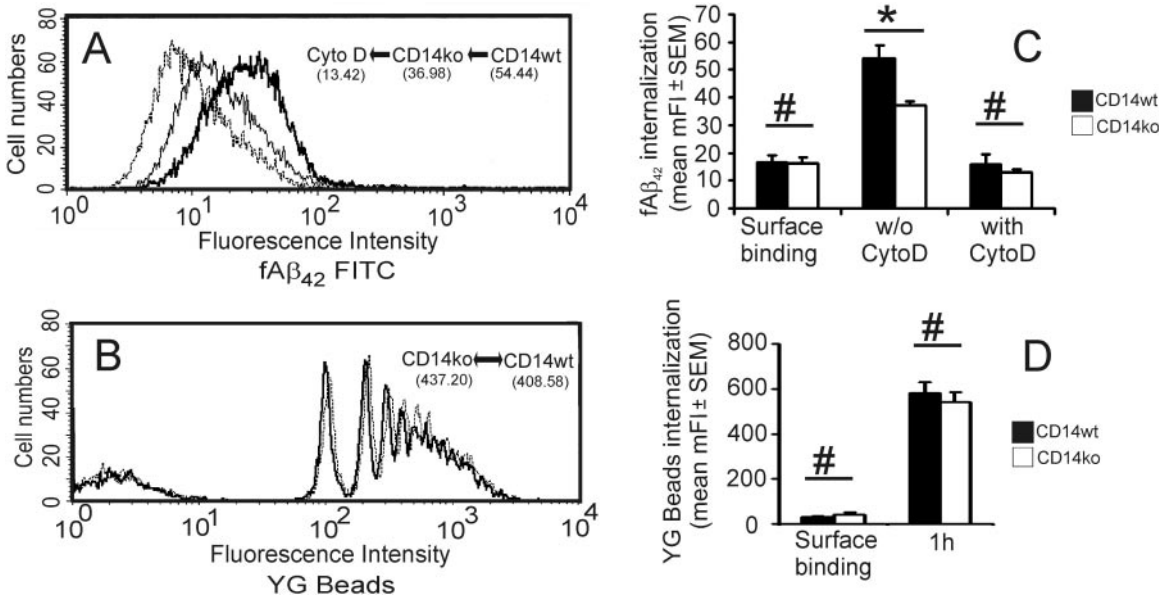

Fig. 6 Quantification of fAβ$_{42}$ and polystyrene microsphere internalization. Overlay of flow cytometry histograms of CD14ko microglia (thin continuous line) and CD14wt microglia (bold continuous line) demonstrates that fluorescence intensity of CD14wt microglia is higher than that of CD14ko microglia after fAβ$_{42}$ internalization (**A**). The increase of fluorescence in CD14wt microglia is aborted after pre-treatment with 2.5 μM cytochalasin D (CytoD; dotted line) (**A**). Internalization of fAβ$_{42}$ as determined by mFI is significantly reduced in CD14ko microglia (open bar) compared with CD14wt microglia (filled bar) (**C**). Overlay of histograms (**B**) shows unchanged fluorescence intensity distribution in CD14ko microglia (dotted line) after the microsphere bead internalization compared with CD14wt cells (continuous line). No significant difference in mFI after the bead internalization between CD14ko (open bar) and CD14wt microglia (filled bar) was observed (**D**). Values of each bar represent mean mFI ± SEM of at least three independent experiments. *$P < 0.05$, $n = 4$; # $P > 0.05$, $n = 3$, independent-samples *t*-test.

transcript levels between CD14ko and CD14wt microglia (data not shown).

fAβ_{42} at concentrations between 0.25 and 2.5 μg/ml does not activate microglial inflammatory and CD14 gene transcription

After establishing that Aβ_{42} fibrils are rapidly internalized into microglia with the help of CD14, we asked whether this internalization is associated with a microglial inflammatory reaction and up-regulation of CD14 transcription that might be induced by Aβ fibrils. We quantified transcripts of inflammatory genes, iNOS and TNF-α, and CD14, after fAβ_{42} treatments in CD14wt microglia. We found that fAβ_{42} at concentrations of 0.25 μg/ml or 2.5 μg/ml did not activate microglial inflammation within 1 h (Fig. 7). However, higher concentrations of Aβ_{42} fibrils (25 μg/ml) up-regulated microglial gene transcripts of iNOS and TNF-α (Fig. 7). Aβ_{42} fibrils at concentrations below 25 μg/ml did not up-regulate the CD14 transcript, but 100 ng/ml LPS did so (Fig. 7).

In order to exclude the possibility that fAβ_{42} at the different concentrations used in this experiment would lead to different conformations of peptides in the culture medium which might cause different microglial inflammatory reactions, we recovered the free Aβ_{42} peptides from the culture medium 1 h after incubation of fAβ_{42} with microglial cells by immunoprecipitation with mouse monoclonal antibody W0-2 (Centre of Molecular Biology, Heidelberg) directed against amino acids 4–10 of human Aβ (Fassbender *et al.*, 2001) and then assessed the aggregation species of Aβ_{42} by western blotting (Dahlgren *et al.*, 2002). We observed the same aggregation species of the recovered Aβ_{42} as those of the originally added fAβ_{42} (data not shown).

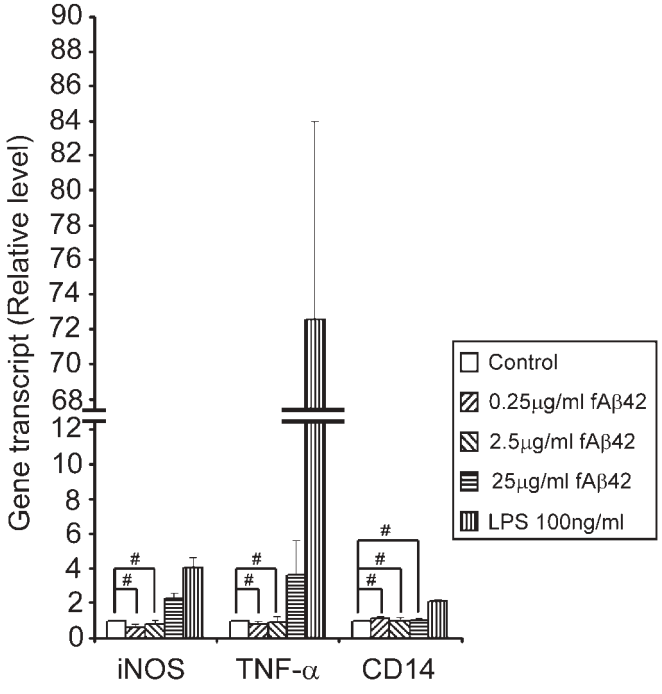

Fig. 7 Microglial inflammatory and CD14 gene transcription after fAβ_{42} treatments. Cultured CD14wt microglia were treated with 0.25, 2.5 and 25 μg/ml fibrillar Aβ_{42} for 1 h. LPS (100 ng/ml, 1 h incubation time) was used as positive control. Gene transcript (mRNA) levels of iNOS, TNF-α and CD14 were measured by real-time PCR after reverse transcription. Within 1 h, fAβ_{42} at 0.25 and 2.5 μg/ml failed to up-regulate iNOS and TNF-α gene transcript levels (# $P > 0.05$, $n = 3$, independent-samples *t*-test), whereas 25 μg/ml fAβ_{42} showed increased levels of iNOS and TNF-α gene transcripts. fAβ_{42} at the concentrations <25 μg/ml did not up-regulate CD14 transcripts (# $P > 0.05$, $n = 3$, independent-samples *t*-test) but LPS did.

CD14 is over-expressed on parenchymal microglia in human Alzheimer's disease brains

We investigated whether CD14 is actually present in the brains of Alzheimer's disease patients. Immunohistochemical staining of brains of Alzheimer's disease patients ($n = 9$) revealed a strong expression of CD14 on microglia diffusing in the parenchyma of frontal and occipital (Fig. 8A–C) cortex, hippocampus (Fig. 8 D) and around some senile plaques where they were located mainly in the area of the neurites surrounding the Aβ deposits. In addition, some perivascular cells showed CD14-positive staining, probably corresponding to macrophages. In contrast, immunohistochemical staining of brains of age-related, non-demented control subjects ($n = 2$) did not show any parenchymal staining, but only showed perivascular macrophage-related positive signals. The presence of CD14 in Alzheimer's disease brains in the pathophysiologically relevant areas further strengthens the argument for a possible role of CD14 in Alzheimer's disease indicated by the experimental results.

Discussion

Vaccination studies in animal models of Alzheimer's disease with Aβ show that Aβ plaques are removed by microglia leading to an amelioration of the cognitive function (Bard *et al.*, 2000; Janus *et al.*, 2000). The exact molecular mechanism by which microglial cells clear Aβ deposits is still unknown. Our results indicate that a key receptor of innate immunity, the LPS receptor CD14, could contribute to this plaque removal: We show that CD14 closely interacts with fibrillar Aβ_{42}, thereby facilitating its internalization by microglia. Our detection of CD14 immunoreactivity spatially correlated with sites of characteristic lesions in Alzheimer's disease patients extends these experimental results to human disease.

CD14 interacts not only with several pathogen-associated molecular patterns (PAMP) (Peterson *et al.*, 1995; Muro *et al.*, 1997; Lipovsky *et al.*, 1997; Poussin *et al.*, 1998), but also with endogenous structures such as atherogenic lipids (Schmitz and Orso, 2002) and apoptotic bodies (Devitt *et al.*, 1998). Using a FLIM-based FRET technique for investigation of the biochemical reactions in living cells, we showed that human

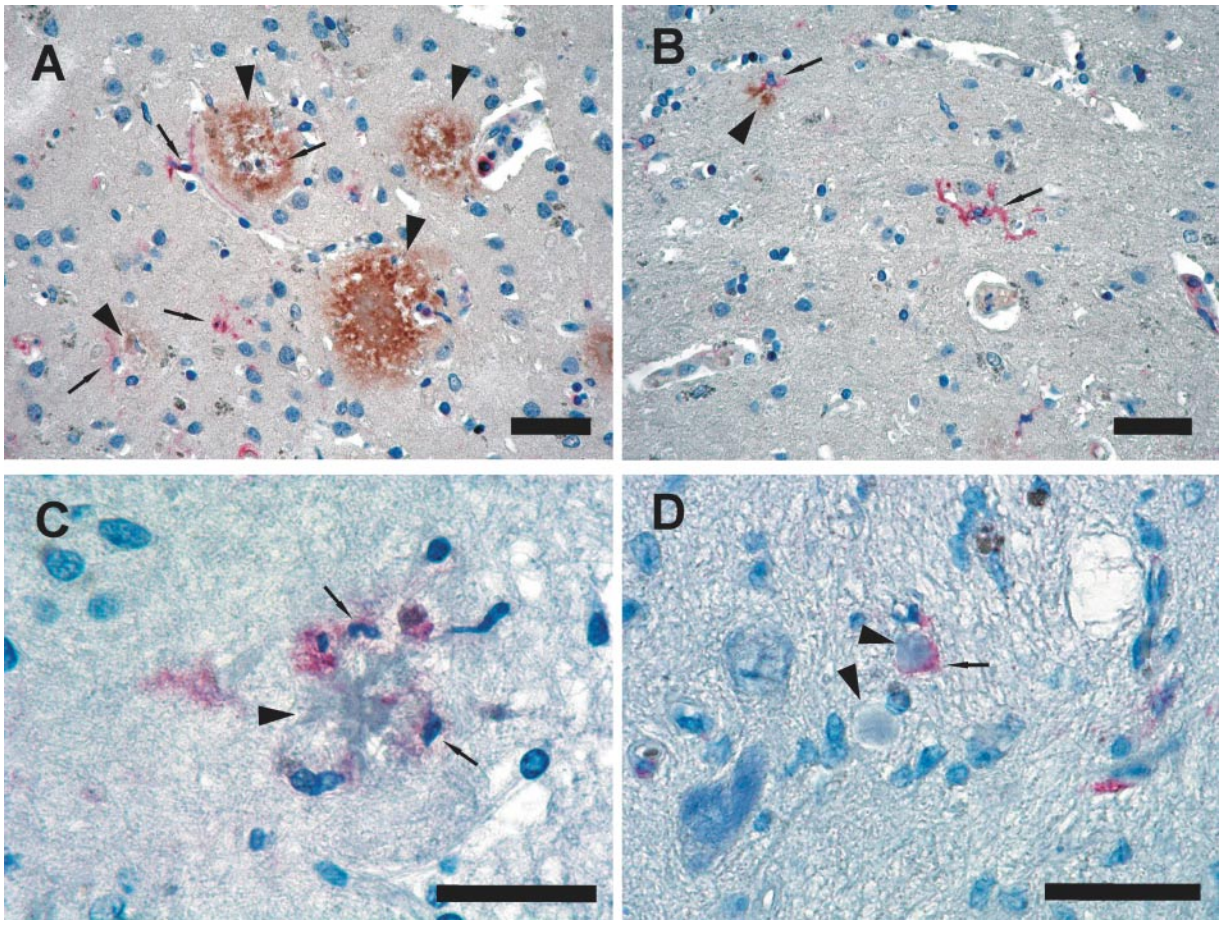

Fig. 8 CD14 overexpression on parenchymal microglia in Alzheimer's disease brains. In occipital cortex (**A**–**C**) and hippocampus (**D**) from different Alzheimer's disease patients, CD14 was strongly expressed as indicated by the red staining on microglial cells (narrow arrow) diffusing in the parenchyma and around some senile plaques (arrow head) as well as on macrophages/microglia in the perivascular space. In the double-staining figures (**A**, **B**), senile plaques were stained brown with anti-Aβ antibody. Microglia clearly surround and stay inside of senile plaques (**A**) and keep a direct contact with Aβ deposits (**B**). Isotype control staining presented no specific immunohistochemical signals. Scale bars: 100 μm.

CD14 interacts with, and in all likelihood directly binds to, $fA\beta_{42}$ both on the cell surface and intracellularly within vesicular-like structures.

We present several lines of evidence supporting our hypothesis that CD14 plays an important role in $A\beta_{42}$ internalization into microglia. First, confocal microscopy analysis revealed that CD14 co-localizes with $fA\beta_{42}$ and facilitates its internalization into microglia in a time- and concentration-dependent manner. Secondly, using confocal microscopy and flow cytometry to quantify the involvement of CD14 in internalization of $fA\beta_{42}$, we observed that CD14-positive microglia ingest significantly more $fA\beta_{42}$ than do those derived from CD14-deficient mice.

Interestingly, in the field of innate immunity, it is well known that CD14 not only facilitates phagocytosis of microbial components (Poussin *et al.*, 1998; Vasselon *et al.*, 1999) but also mediates cellular inflammatory activation (Haziot *et al.*, 1996). Previously, we demonstrated that CD14 is able to mediate cellular inflammatory activation by $A\beta_{42}$ (Fassbender *et al.*, 2004). These findings were considerably strengthened by a subsequent study that showed that anti-CD14 strategies (e.g. CD14-IgG chimera) reduce neurotoxicity of Aβ-stimulated microglia (Bate *et al.*, 2004). The need for the host cells to combat invading pathogens both by phagocytosis of pathogens and by release of cytotoxic products (Aderem, 2003; Blander and Medzhitov, 2004) may explain such a dual function of CD14 and other receptors, including scavenger receptor class B type I (Bocharov *et al.* 2004), Fc receptor (Ravetch and Clynes, 1998) and complement receptor 3 (Le Cabec *et al.*, 2002). However, in Alzheimer's disease pathophysiology, CD14 may function as a two-edged sword: its role in phagocytosis is considered to be beneficial whereas its role in cellular activation and release of neurotoxic products is assumed to be detrimental.

Notably, concentrations for internalization were 10× lower than those previously shown in our studies and those by others to be needed to activate microglia (Meda *et al.*, 1995; Fassbender *et al.*, 2004). We propose that phagocytosis might be dissociated from inflammatory microglial activation in relation to the Alzheimer's disease stage. For example,

at low (500 nM) Aβ concentrations (corresponding to those observed in the brain of early or middle stage of Alzheimer's disease) (Schenk *et al.*, 1999), CD14 may only mediate phagocytosis, whereas at higher Aβ concentrations (corresponding to those found in brains of late stage of Alzheimer's disease), CD14 may confer cellular activation resulting in production of neurotoxins as well.

Several receptors have been reported to be possibly engaged in Aβ clearance. Scavenger receptors phagocytose aggregated Aβ (Paresce *et al.*, 1996); however, since the genetic deficiency of the scavenger receptor affected neither Aβ deposition nor synaptic degeneration in amyloid precursor protein (APP) overexpressing mice (Huang *et al.*, 1999), additional receptors could be involved in Aβ phagocytosis. Formyl peptide receptor-like 1 (FPRL1) has been shown to co-localize with Aβ during the peptide internalization by macrophages (Yazawa *et al.*, 2001), although direct involvement of FPRL1 in Aβ uptake has not been shown. The Fc receptor has also been considered to mediate Aβ clearance by microglia after passive transfer of anti-Aβ antibodies (Bard *et al.*, 2000). However, $A\beta_{42}$ immunization attenuated Aβ deposition regardless of whether or not the mice were genetically deficient for the Fc receptor (Das *et al.*, 2003). Finally, complement receptors that are consistently found in plaques in Alzheimer's disease brains (Eikelenboom and Veerhuis, 1996) are also able to facilitate clearance of opsonized Aβ. Indeed, inhibition of complement 3 in a mouse model of Alzheimer's disease increased plaque formation and neurodegeneration (Wyss-Coray *et al.*, 2002). It is highly likely that CD14 is a major receptor for Aβ phagocytosis, and that several receptors, rather than only one, collaborate in microglial phagocytosis of Aβ.

In complementary histopathological studies, we were able to detect CD14-immunoreactive parenchymal microglia in brains of Alzheimer's disease patients but not in those of control subjects. The microglia over-expressing CD14 mainly diffuse in the parenchyma and surround some senile plaques, which suggests that CD14-overexpressing microglia possibly respond to premature Aβ deposits or newly formed senile plaques. This is also suggested by the observation that, in APP transgenic mice, the number and size of amyloid β deposits increase with aging (Sturchler-Pierrat *et al.*, 1997). The observation that CD14 microglia, in contrast to (HLA)-DR-immunoreactive microglia (Itagaki *et al.*, 1989), were not present in all compact-Aβ deposits, suggests that CD14 immunoreactive microglia represent only one subtype of microglia. Additionally, it has been reported that the density of CD68-immunoreactive microglia correlates with amyloid β plaques in the early stage but not in the late stage of Alzheimer's disease (Arends *et al.*, 2000). Therefore, CD14 may be a marker for a more phagocytic subtype of microglia, which could explain our *in vitro* findings. This correlation between CD14 immunoreactivity and characteristic Alzheimer's disease lesion sites extends the experimental results to a clinical level, further supporting a possible involvement of CD14 in human disease.

In summary, the results of this study demonstrate that the LPS receptor CD14 interacts with Aβ fibrils and thereby contributes to microglial phagocytosis of $A\beta_{42}$ fibrils. These findings, together with the first demonstration of CD14 expression in brains of Alzheimer's disease patients, suggest a pathophysiologically and possibly therapeutically relevant role of CD14 in Alzheimer's disease.

Acknowledgements

We wish to thank Laura Swan for her careful reading of the manuscript. This work was supported by the University of Göttingen, DFG Research Centre for Molecular Physiology of the Brain (to K.F.) grants from the Deutsche Forschungsgemeinschaft Fa212/3–2,3 (to K.F.), BMBF-Schwerpunkt TSE-Therapie (to K.F.), European Union QLRT-1999–02004 (to K.F.) and Hertie-Foundation (M.S. and H.N.). The monoclonal antibody (ABL-93) developed by J. T. August was obtained from the Development Studies Hybridoma Bank (DSHB) developed under the auspices of the US National Institute of Child Health and Human Development (NICHD) and maintained by the University of Iowa, Department of Biological Sciences, Iowa City, IA 52242, USA.

References

Aderem A. Phagocytosis and the inflammatory response. J Infect Dis 2003; 187 Suppl 2: S340–5.

Akiyama H, McGeer PL. Specificity of mechanisms for plaque removal after Aβ immunotherapy for Alzheimer disease. Nat Med 2004; 10: 117–8.

Arends YM, Duyckaerts C, Rozemuller JM, Eikelenboom P, Hauw JJ. Microglia, amyloid and dementia in Alzheimer's disease. A correlative study. Neurobiol Aging 2000; 21: 39–47.

Bacskai BJ, Skoch J, Hickey GA, Allen R, Hyman BT. Fluorescence resonance energy transfer determinations using multiphoton fluorescence lifetime imaging microscopy to characterize amyloid-beta plaques. J Biomed Optics 2003; 8: 368–75.

Bard F, Cannon C, Barbour R, Burke RL, Games D, Grajeda H, et al. Peripherally administered antibodies against amyloid beta-peptide enter the central nervous system and reduce pathology in a mouse model of Alzheimer disease. Nat Med 2000; 6: 916–9.

Bate C, Veerhuis R, Eikelenboom P, Williams A. Microglia kill amyloid-beta1-42 damaged neurons by a CD14-dependent process. Neuroreport 2004; 15: 1427–30.

Blander JM, Medzhitov R. Regulation of phagosome maturation by signals from toll-like receptors. Science 2004; 304: 1014–18.

Bocharov AV, Baranova IN, Vishnyakova TG, Remaley AT, Csako G, Thomas F, et al. Targeting of scavenger receptor class B type I by synthetic amphipathic alpha-helical-containing peptides blocks lipopolysaccharide (LPS) uptake and LPS-induced pro-inflammatory cytokine responses in THP-1 monocyte cells. J Biol Chem 2004; 279: 36072–82.

Borchardt T, Camakaris J, Cappai R, Masters CL, Beyreuther K, Multhaup G. Copper inhibits β-amyloid production and stimulates the non-amyloidogenic pathway of amyloid-precursor-protein secretion. Biochem J. 1999; 344 Pt 2: 461–7.

Check E. Nerve inflammation halts trial for Alzheimer's drug. Nature 2002; 415: 462.

Chen JW, Murphy TL, Willingham MC, Pastan I, August JT. Identification of two lysosome membrane glycoproteins. J Cell Biol 1985; 101: 85–95.

Citron M. Alzheimer's disease: treatments in discovery and development. Nat Neurosci 2002; 5 Suppl: 1055–7.

Dahlgren KN, Manelli AM, Stine WB Jr, Baker LK, Krafft GA, LaDu MJ. Oligomeric and fibrillar species of amyloid-beta peptides differentially affect neuronal viability. J Biol Chem 2002; 277: 32046–53.

Das P, Howard V, Loosbrock N, Dickson D, Murphy MP, Golde TE. Amyloid-beta immunization effectively reduces amyloid deposition in FcRgamma-/- knock-out mice. J Neurosci 2003; 23: 8532–8.

Devitt A, Moffatt OD, Raykundalia C, Capra JD, Simmons DL, Gregory CD. Human CD14 mediates recognition and phagocytosis of apoptotic cells. Nature 1998; 392: 505–9.

Eikelenboom P, Veerhuis R. The role of complement and activated microglia in the pathogenesis of Alzheimer's disease. Neurobiol Aging 1996; 17: 673–80.

Fassbender K, Simons M, Bergmann C, Stroick M, Lutjohann D, Keller P, et al. Simvastatin strongly reduces levels of Alzheimer's disease beta -amyloid peptides Aβ 42 and Aβ 40 *in vitro* and *in vivo*. Proc Natl Acad Sci USA 2001; 98: 5856–61.

Fassbender K, Walter S, Kuhl S, Landmann R, Ishii K, Bertsch T, et al. The LPS receptor (CD14) links innate immunity with Alzheimer's disease. FASEB J 2004; 18: 203–5.

Games D, Adams D, Alessandrini R, Barbour R, Berthelette P, Blackwell C, et al. Alzheimer-type neuropathology in transgenic mice overexpressing V717F beta-amyloid precursor protein. Nature 1995; 373: 523–7.

Golenbock DT, Liu Y, Millham FH, Freeman MW, Zoeller RA. Surface expression of human CD14 in Chinese hamster ovary fibroblasts imparts macrophage-like responsiveness to bacterial endotoxin. J Biol Chem 1993; 268: 22055–9.

Haziot A, Ferrero E, Kontgen F, Hijiya N, Yamamoto S, Silver J, et al. Resistance to endotoxin shock and reduced dissemination of gram-negative bacteria in CD14-deficient mice. Immunity 1996; 4: 407–14.

Hoyer W, Antony T, Cherny D, Heim G, Jovin TM, Subramaniam V. Dependence of alpha-synuclein aggregate morphology on solution conditions. J Mol Biol 2002; 322: 383–93.

Huang F, Buttini M, Wyss-Coray T, McConlogue L, Kodama T, Pitas RE, et al. Elimination of the class A scavenger receptor does not affect amyloid plaque formation or neurodegeneration in transgenic mice expressing human amyloid protein precursors. Am J Pathol 1999; 155: 1741–47.

Ishii K, Muelhauser F, Liebl U, Picard M, Kuhl S, Penke B, et al. Subacute NO generation induced by Alzheimer's beta-amyloid in the living brain: reversal by inhibition of the inducible NO synthase. FASEB J 2000; 14: 1485–9.

Itagaki S, McGeer PL, Akiyama H, Zhu S, Selkoe D. Relationship of microglia and astrocytes to amyloid deposits of Alzheimer disease. J Neuroimmunol. 1989; 24: 173–82.

Janus C, Pearson J, McLaurin J, Mathews PM, Jiang Y, Schmidt SD, et al. A beta peptide immunization reduces behavioural impairment and plaques in a model of Alzheimer's disease. Nature 2000; 408: 979–82.

Katoh S, Zheng Z, Oritani K, Shimozato T, Kincade PW. Glycosylation of CD44 negatively regulates its recognition of hyaluronan. J Exp Med 1995; 182: 419–9.

Le Cabec V, Carreno S, Moisand A, Bordier C, Maridonneau-Parini I. Complement receptor 3 (CD11b/CD18) mediates type I and type II phagocytosis during nonopsonic and opsonic phagocytosis, respectively. J Immunol 2002; 169: 2003–9.

Lipovsky MM, Gekker G, Anderson WR, Molitor TW, Peterson PK, Hoepelman AI. Phagocytosis of nonopsonized Cryptococcus neoformans by swine microglia involves CD14 receptors. Clin Immunol Immunopathol 1997; 84: 208–11.

McGeer EG, McGeer PL. Inflammatory processes in Alzheimer's disease. Prog Neuropsychopharmacol Biol Psychiatry 2003; 27: 741–9.

Meda L, Cassatella MA, Szendrei GI, Otvos L Jr, Baron P, Villalba M, et al. Activation of microglial cells by beta-amyloid protein and interferon-gamma. Nature 1995; 374: 647–50.

Mimura N, Asano A. Synergistic effect of colchicine and cytochalasin D on phagocytosis by peritoneal macrophages. Nature 1976; 261: 319–21.

Moore KJ, Andersson LP, Ingalls RR, Monks BG, Li R, Arnaout MA, et al. Divergent response to LPS and bacteria in CD14-deficient murine macrophages. J Immunol 2000; 165: 4272–80.

Muro M, Koseki T, Akifusa S, Kato S, Kowashi Y, Ohsaki Y, et al. Role of CD14 molecules in internalization of Actinobacillus actinomycetemcomitans by macrophages and subsequent induction of apoptosis. Infect Immun 1997; 65: 1147–51.

Nicoll JA, Wilkinson D, Holmes C, Steart P, Markham H, Weller RO. Neuropathology of human Alzheimer disease after immunization with amyloid-beta peptide: a case report. Nat Med 2003; 9: 448–52.

Paresce DM, Ghosh RN, Maxfield FR. Microglial cells internalize aggregates of the Alzheimer's disease amyloid beta-protein via a scavenger receptor. Neuron 1996; 17: 553–65.

Peterson PK, Gekker G, Hu S, Sheng WS, Anderson WR, Ulevitch RJ, et al. CD14 receptor-mediated uptake of nonopsonized Mycobacterium tuberculosis by human microglia. Infect Immun 1995; 63: 1598–602.

Poussin C, Foti M, Carpentier JL, Pugin J. CD14-dependent endotoxin internalization via a macropinocytic pathway. J Biol Chem 1998; 273: 20285–91.

Ravetch JV, Clynes RA. Divergent roles for Fc receptors and complement *in vivo*. Annu Rev Immunol 1998; 16: 421–32.

Schenk D, Barbour R, Dunn W, Gordon G, Grajeda H, Guido T, et al. Immunization with amyloid-beta attenuates Alzheimer-disease-like pathology in the PDAPP mouse. Nature 1999; 400: 173–7.

Schmitz G, Orso E. CD14 signalling in lipid rafts: new ligands and co-receptors. Curr Opin Lipidol 2002; 13: 513–21.

Sturchler-Pierrat C, Abramowski D, Duke M, Wiederhold KH, Mistl C, Rothacher S, et al. Two amyloid precursor protein transgenic mouse models with Alzheimer disease-like pathology. Proc Natl Acad Sci USA 1997; 94: 13287–92.

Stryer L. Fluorescence Energy Transfer as a Spectroscopic Ruler. Ann Rev Biochem 1978; 17: 819–46.

Vasselon T, Hailman E, Thieringer R, Detmers PA. Internalization of monomeric lipopolysaccharide occurs after transfer out of cell surface CD14. J Exp Med 1999; 190: 509–21.

Wyss-Coray T, Yan F, Lin AH, Lambris JD, Alexander JJ, Quigg RJ, et al. Prominent neurodegeneration and increased plaque formation in complement-inhibited Alzheimer's mice. Proc Natl Acad Sci USA 2002; 99: 10837–42.

Yazawa H, Yu ZX, Takeda, Le Y, Gong W, Ferrans VJ, et al. Beta amyloid peptide (Aβ42) is internalized via the G-protein-coupled receptor FPRL1 and forms fibrillar aggregates in macrophages. FASEB J 2001; 15: 2454–62.